*J. Fluid Mech.*, page 1 of 27. © Cambridge University Press 2012
doi:10.1017/jfm.2012.364


# The surface signature of internal waves

**W. Craig[1]†, P. Guyenne[2] and C. Sulem[3]**

[1] Department of Mathematics and Statistics, McMaster University, Hamilton, ON, L8S 4K1, Canada
[2] Department of Mathematical Sciences, University of Delaware, DE 19716, USA
[3] Department of Mathematics, University of Toronto, ON, M5S 3G3, Canada

(Received 17 January 2012; revised 15 May 2012; accepted 16 July 2012)

Oceans that are stratified by density into distinct layers support internal waves. An internal soliton gives rise to characteristic features on the surface, a signature of its presence, in the form of a 'rip' region, as reported in Osborne & Burch (*Science*, vol. 208, 1980, pp. 451–460), which results in a change in reflectance as seen in NASA photographs from the space shuttle. In the present paper, we give a new analysis of this signature of an internal soliton, and the 'mill pond' effect of an almost completely calm sea after its passage. Our analysis models the resonant interaction of nonlinear internal waves with the surface modes, where the surface signature is generated by a process analogous to radiative absorption. These theoretical results are illustrated with numerical simulations that take oceanic parameters into account.

**Key words:** Hamiltonian theory, internal waves, surface gravity waves

## 1. Introduction

Internal waves occur within a fluid that is density-stratified, most commonly by temperature or salinity variation. In the oceans, such disturbances in internal layers are often generated by tides. The combination of local and remote sensing observations, as well as the progress in detection technology over the last 40 years, have shown that internal soliton-like waves are common and important features of oceans in many regions of the world. On the practical side, internal waves are important to mixing processes in oceans, they can have an influence on measurements of current and on undersea navigation, and they present a potential hazard for offshore platforms. A recent survey article by Helfrich & Melville (2006) gives an overview of properties of internal solitary waves, with a comprehensive bibliography.

Among the early measurements were those of Perry & Schimke (1965), which found groups of internal waves with amplitudes of up to 80 m, wavelengths of 2000 m, on the main thermocline situated at 500 m in water 1500 m deep in the Andaman Sea. Photographs taken from the orbiting space shuttle (see e.g. an extensive collection of images at http://www.internalwaveatlas.com) display a characteristic change in the reflectance of the surface wave pattern, a signature due to the presence of rough waters sometimes referred to as 'rip', on the free surface travelling above an internal wave. Osborne & Burch (1980) describe the passage of this rip in a striking sequence of photographs taken from shipboard, including the resulting complete calmness of the sea after its passage, the 'mill pond' effect. In this article, we describe the rip

† Email address for correspondence: craig@math.mcmaster.ca

region of the free surface as being generated by the resonant coupling between internal solitons and the free-surface wave mode. Furthermore, we give an explanation of the mill pond effect as the result of a dominant reflection coefficient for free-surface waves in the modulational regime, in a frame of reference moving with the internal soliton.

There is a large literature on the problem of interaction between internal and surface waves, which can roughly be subdivided into three types: studies that consider interactions between internal waves and surface waves of comparable length scales (e.g. Gear & Grimshaw 1984; Părău & Dias 2001), studies of resonant interactions between internal and surface waves of substantially different length scales (e.g. Kawahara, Sugimoto & Kakutani 1975; Hashizume 1980; Funakoshi & Oikawa 1983; Ma 1983), and studies of the deformation of a surface wave field due to a given underlying current. Contributions of the second type are closest in nature to the present work, deriving model equations for the case of resonant internal mode–surface mode interactions. However, their principal focus has been the derivation of coupled model equations for surface and internal waves, and the authors are less concerned with the nature of the surface signature. Because of its complexity, most theoretical studies that address the question of the surface signature of an internal wave are of the third type, modelling the surface manifestation of an internal wave indirectly through the action on surface waves of a specified current that the internal wave is assumed to induce. These are ray-based theories, which are widely followed in applications to the remote sensing of internal waves via their surface signature, using phase-averaged models based on either a wave energy balance equation incorporating radiation stresses (e.g. Gargett & Hughes 1972; Lewis, Lake & Ko 1974), or a wave action balance equation combined with ray theory (e.g. Caponi *et al.* 1988; Bakhanov & Ostrovsky 2002). In this framework, surface waves are described statistically by a density function, while the effects of an internal wave are represented by a near-surface current with a prescribed form. The existence of the rip is taken to be the result of wavenumber upshift in regions of a converging current induced by a passing internal wave. Furthermore, because of this tendency of surface waves to shorten and steepen in these regions, an explanation of the mill pond effect is that they are thus more likely to break, leaving calmer water after the internal wave passage (Phillips 1966). Indeed, direct numerical simulations by Donato, Peregrine & Stocker (1999) clearly show the focusing and near-breaking of short surface waves due to a sinusoidal current.

However, a number of aspects of the phenomenon of surface rips as signatures of internal waves, and the mill pond effect after their passage, are not fully described by the above theories. One is the characteristic narrowness of the rip, which contrasts with the known phenomenon of broadening of large-amplitude internal solitons. A second is a precise description of the surface current that is induced by the passage of an internal solitary wave. A third is the location of the rip with respect to the centre of an internal solitary wave. A fourth has to do with the quantitative question as to whether the energy decrease that is evident in the smoothing of the surface wave fields in the mill pond effect is sufficiently accounted for by dissipation due to wave breaking in the rip region. The present paper addresses all four of these issues, based on a reassessment of the modelling, the analysis and the interpretation of phenomena in the problem of internal–surface wave interactions. Specific features of our reassessment include the following.

(i) Our approach models explicitly the resonant interaction of internal and surface waves in a physically relevant scaling regime, namely long internal waves

interacting with modulated quasi-monochromatic surface waves. There are two cases in our analysis, determined by the scaling relationship between the internal mode and the free-surface mode. The first of these cases corresponds to nonlinear interactions between the internal modes and the free-surface modes, where surface waves drive internal wave motion and vice versa. The second case corresponds to a fully developed nonlinear internal wave underlying a relatively more quiescent ambient sea surface. In either case, the resulting system describes the evolution of the internal mode with a Korteweg–de Vries (KdV) equation, coupled to a Schrödinger equation for the modulation of the free surface. These dynamics are fully deterministic. The first case is the subject of the articles by Kawahara *et al.* (1975) and Hashizume (1980), which derive model equations similar to our own; these papers, however, do not discuss the size of the nonlinear coupling coefficients, nor do they give an analysis of the phenomenon of a surface signature. In the present article, we principally study the second case, and we focus in particular on the formation of the surface signature rip, and the phenomenon of the mill pond effect. Furthermore, in our analysis, we adopt a Hamiltonian formulation of the problem, which implies that both wave action and energy are invariants of motion. In our view, this is a higher level of approximation than the aforementioned previous approaches, which model the effects of internal waves using a steady current whose form is adjusted to fit observations. Our approach differs from, for example, the concept of radiation stress in which energy is not conserved (Longuet-Higgins & Stewart 1964), and from arguments invoking dissipation by wave breaking. We are also addressing a different scaling regime for interface–free surface interactions than the studies by Funakoshi & Oikawa (1983) and Ma (1983), who consider the case in which the amplitudes of surface waves dominate those of the internal waves.

(ii) Our model equations are derived directly from a mathematical formulation for two-layer flows with a free surface and, as a result, the coefficients in these equations (and hence their solutions) depend explicitly on physical parameters of the two-layer system (see appendix B). This explicit dependence allows for a detailed parametric analysis of our results in realistic situations, in particular in the case of small density differences between fluid layers or small mean depth ratios. In an analogy with quantum mechanics, this regime of parameters corresponds to the semi-classical limit of the Schrödinger equation for which the potential is a well (i.e. an internal soliton of depression) and the non-dimensional coefficient of dispersion is very small. It is representative of internal waves evolving, for example, in coastal seas (Helfrich & Melville 2006). Lee *et al.* (2007) also derived a linear Schrödinger equation for the modulation of surface waves by internal waves but, again, they only considered a one-layer system in which the internal waves are modelled by a prescribed current.

(iii) The resonant excitation of quasi-monochromatic surface waves whose group velocity coincides with the phase velocity of long internal waves has been reported in many observations (e.g. Lewis *et al.* 1974; Osborne & Burch 1980). A similar resonance phenomenon between gravity and capillary wave modes in a free surface is described by Djordjevic & Redekopp (1977), whose model equations for the phenomenon are very similar to those of Funakoshi & Oikawa (1983). In the present case, the resonance condition comes out naturally as part of the reduction of the Hamiltonian system (see (3.6)), which can be viewed as a two-layer generalization of the commonly used one-layer condition involving the linear dispersion relation of deep-water surface waves. The resonance is

typically between two wavenumbers of greatly differing magnitude. Our numerical solutions of (3.6) confirm that this resonance typically occurs for surface waves whose characteristic wavelength is much shorter than the internal wavelength scale.

(iv) Our theoretical picture relates the surface modulation of waves advected by fluid motion induced by internal waves to bound states of a linear Schrödinger equation with a potential well given by an internal soliton. Wave energy from the sea surface is trapped by these bound states during the internal wave passage, which gives rise to the phenomenon of a region of rip. In the setting of interest (i.e. the semi-classical regime), these bound states are known to be very localized in space. This is consistent with observations that the rip usually appears as narrow bands of rough water separated by larger areas of calm water, as shown, for example, on aerial or satellite images (Gargett & Hughes 1972; Alpers 1985; Gasparovic, Apel & Kasischke 1988). This close resemblance is partly due to the fact that our approach takes into account an accurate representation of the local currents induced by an internal wave through a precise asymptotic analysis of the Dirichlet–Neumann operator and an exact solution of the KdV equation with physically relevant parameters, a replacement for the role of a predefined current in the previous analyses. Numerical simulations showing details of the rip pattern in oceanic conditions are presented in figures 5 and 6. We also use exact solutions of the KdV equation to give an estimate for the narrowness of the rip region, and to derive an estimate for the rate of wave energy absorption into bound states. This picture is consistent with the images of rip regions in the NASA images of internal waves, where it is common to have a very uniform character of the rip over a large lateral span. These observations contrast with the ray theoretic explanations of the rip region, for which the character depends specifically on the local details of the ambient sea state through which the internal wave is moving. Indeed, a criticism of over-reliance on the ray theory is that the resulting systematic distortion of an ambient wave pattern by a current depends significantly on the character of the wave pattern itself. This is described in detail in Basovich & Talanov (1977) and Basovich & Bahanov (1984) in the context of geometrical optics. Physical observations of rip regions, however, show a remarkable similarity of the rip structure over sometimes hundreds of kilometres of lateral extent, while ray theory alone would predict that non-uniformities of the ambient sea state over this large area would be seen in the rip pattern. Our own theory leads to the prediction that a closer Fourier analysis of the rip region will show a more uniform pattern with a dominant carrier wavenumber, indeed the resonant wavenumber for the internal mode–surface mode interaction.

(v) Finally we show that the reflection and transmission coefficients, $b(k)$ and $c(k)$ respectively, for the solution of the Schrödinger equation in the semi-classical regime are asymptotic to $b = -1$ and $c = 0$ for a range of sideband wavenumbers $k$ near zero. This supports the following compelling explanation of the mill pond effect. In the reference frame of the internal soliton entering a background sea state, quasi-monochromatic surface waves are absorbed into the rip as bound states, or else they are effectively reflected in front of it. The fact that very little of the surface sea state is transmitted through the soliton region gives rise to the region of remarkable calm behind the advancing internal soliton. This contrasts again with the ray methods mentioned above, which explain the mill pond effect in terms of energy loss by wave breaking in the rip zone, a dissipative and highly nonlinear mechanism, and one that is difficult to quantify. In our picture, the mill

pond effect is the result of a conservative and linear mechanism of absorption and reflection of surface wave energy, as described by scattering theory for the linear Schrödinger equation, which does not depend upon energy loss due to wave breaking or other dissipative mechanisms. This explanation is compatible with many observations (e.g. Gargett & Hughes 1972; Osborne & Burch 1980; Bourgault & Kelley 2003) in which no significant and widespread wave breaking is discernible. For the SAR Internal Wave Signature Experiment (SARSEX) in the New York Bight, Gasparovic *et al.* (1988) reported breaking wave events only under high wind conditions, which also suggests that the rip phenomenon and hence the mill pond effect are not necessarily associated with wave breaking.

The starting point of our study is the Euler equations of motion for an incompressible irrotational fluid composed of two immiscible layers of different densities. In § 2, we write the Hamiltonian formulation of this problem and the corresponding canonical variables. A linear analysis near the fluid at rest provides a normal mode decomposition that identifies the interacting modes. In § 3, we set the scaling regime adapted to the physical situation and perform a sequence of canonical transformations, through which we derive the resonance condition together with the asymptotic coupled system describing the evolution of the internal and free-surface waves. In § 4, we analyse solutions of the coupled system, and the influence of relative depth in the realistic case of density ratio close to unity. The KdV soliton solution for internal waves is derived and discussed. For small Atwood number and/or depth ratios, bound states for the free-surface mode are computed and their properties of radiative absorption are estimated. Furthermore, we calculate the asymptotic values of the reflection and transmission coefficients through the soliton. Concluding remarks are given in § 5, and mathematical details of our derivations and calculations are provided in the appendices.

## 2. Formulation of the problem

Our starting point is the Euler equations of motion for an incompressible, irrotational fluid composed of two immiscible layers of different densities.

### 2.1. *Euler equations for stratified fluids*

The fluid domain is composed of two regions: the lower region $S(\eta) = \{x \in \mathbb{R}, -h < y < \eta(x,t)\}$ and the upper one $S_1(\eta,\eta_1) = \{x \in \mathbb{R}, \eta(x,t) < y < h_1 + \eta_1(x,t)\}$. They are separated by a dynamic interface $\{y = \eta(x,t)\}$. The lower region is bounded below by a rigid bottom located at a constant depth $\{y = -h\}$, while the upper region is bounded above by a free surface $\{y = h_1 + \eta_1(x,t)\}$. Each region is occupied by an immiscible fluid, with $\rho_1$ and $\rho > \rho_1$ being the densities of the upper and lower fluids, respectively. The parameters $h$ and $h_1$ are the mean depths of the lower and upper fluids, respectively. We assume that $h$ is finite, although this is not an inherent restriction of our approach. Taking the fluid motion to be potential flow in regions away from the interface, the velocity is given in the different fluid regions by $\boldsymbol{u}(x,y,t) = \boldsymbol{\nabla}\varphi(x,y,t)$ in $S(\eta)$ and $\boldsymbol{u}_1(x,y,t) = \boldsymbol{\nabla}\varphi_1(x,y,t)$ in $S_1(\eta,\eta_1)$. The governing equations for the potentials are

$$\Delta\varphi = 0 \quad \text{in the domain } S(\eta), \tag{2.1a}$$

$$\Delta\varphi_1 = 0 \quad \text{in the domain } S(\eta,\eta_1). \tag{2.1b}$$

The boundary condition on the fixed bottom of the lower fluid is

$$\partial_y\varphi = 0 \quad \text{on } y = -h. \tag{2.2}$$

On the interface $y = \eta(x, t)$, we impose three boundary conditions, two of them being kinematic and the third one being the Bernoulli condition of balance of forces,

$$\partial_t \eta + \partial_x \eta \, \partial_x \varphi - \partial_y \varphi = 0, \tag{2.3}$$

$$\partial_t \eta + \partial_x \eta \, \partial_x \varphi_1 - \partial_y \varphi_1 = 0, \tag{2.4}$$

$$\rho(\partial_t \varphi + \tfrac{1}{2} |\nabla \varphi|^2 + g\eta) - \rho_1(\partial_t \varphi_1 + \tfrac{1}{2} |\nabla \varphi_1|^2 + g\eta) = 0, \tag{2.5}$$

where $g$ is the acceleration due to gravity. Finally, on the upper surface $y = h_1 + \eta_1(x, t)$, the velocity potential and the upper surface satisfy the kinematic and Bernoulli conditions

$$\partial_t \eta_1 + \partial_x \eta_1 \, \partial_x \varphi_1 - \partial_y \varphi_1 = 0, \tag{2.6}$$

$$\partial_t \varphi_1 + \tfrac{1}{2} |\nabla \varphi_1|^2 + g\eta_1 = 0. \tag{2.7}$$

### 2.2. *Hamiltonian formulation*

Zakharov's Hamiltonian formulation of the water wave problem was extended to the case of stratified fluid by Benjamin & Bridges (1997), and expressed in terms of Dirichlet–Neumann operators by Craig, Guyenne & Kalisch (2005). The canonical conjugate variables involve the free boundaries $\eta$ and $\eta_1$ as well as the dependent variables $\xi$ and $\xi_1$ constructed from the traces of the velocity potentials on the interface and surface, namely

$$\xi(x, t) = \rho\varphi(x, \eta(x, t), t) - \rho_1 \varphi_1(x, \eta(x, t), t), \tag{2.8a}$$

$$\xi_1(x, t) = \rho_1 \varphi_1(x, h_1 + \eta_1(x, t), t). \tag{2.8b}$$

In terms of these new variables, equations (2.1)–(2.7) can be expressed as a Hamiltonian system in the canonical form

$$\partial_t \begin{pmatrix} \eta \\ \xi \\ \eta_1 \\ \xi_1 \end{pmatrix} = \begin{pmatrix} 0 & 1 & 0 & 0 \\ -1 & 0 & 0 & 0 \\ 0 & 0 & 0 & 1 \\ 0 & 0 & -1 & 0 \end{pmatrix} \begin{pmatrix} \delta_\eta H \\ \delta_\xi H \\ \delta_{\eta_1} H \\ \delta_{\xi_1} H \end{pmatrix}, \tag{2.9}$$

whose Hamiltonian $H$ is the sum of the kinetic and potential energies. The kinetic energy is the weighted sum of the Dirichlet integrals associated with the velocity potentials

$$K = \frac{1}{2} \int\int_{-h}^{\eta(x)} \rho \, |\nabla \varphi(x, y)|^2 \, \mathrm{d}y \, \mathrm{d}x + \frac{1}{2} \int\int_{\eta(x)}^{h_1 + \eta_1(x)} \rho_1 \, |\nabla \varphi_1(x, y)|^2 \, \mathrm{d}y \, \mathrm{d}x, \tag{2.10}$$

and the potential energy is

$$V = \frac{1}{2} \int g(\rho - \rho_1) \eta^2(x) \, \mathrm{d}x + \frac{1}{2} \int g\rho_1 [(h_1 + \eta_1)^2(x) - h_1^2] \, \mathrm{d}x. \tag{2.11}$$

Hereinafter, it is understood that the domain of integration in $x$ is $\mathbb{R}$. As detailed in Craig *et al.* (2005), the Dirichlet integrals in (2.10) can be rewritten in terms of the canonical variables through Dirichlet–Neumann operators. The Dirichlet–Neumann operator for the lower domain is defined by

$$G(\eta)\varphi(x, \eta(x, t), t) = \sqrt{1 + (\partial_x \eta)^2} \, \nabla \varphi \cdot \boldsymbol{n}|_{y=\eta}. \tag{2.12}$$

For the upper fluid, the traces of the velocity potential $\varphi_1$ on the free interface given by $\eta$ and the free surface that is defined by $\eta_1$ contribute to the exterior unit normal

derivative of $\varphi_1$ on each boundary. In this case, the Dirichlet–Neumann operator is a matrix operator that takes the form

$$\begin{pmatrix} G_{11} & G_{12} \\ G_{21} & G_{22} \end{pmatrix} \begin{pmatrix} \varphi_1(x, \eta(x,t), t) \\ \varphi_1(x, h_1 + \eta_1(x,t), t) \end{pmatrix} = \begin{pmatrix} -\sqrt{1 + (\partial_x \eta)^2}\, \nabla \varphi_1 \cdot \boldsymbol{n}|_{y=\eta} \\ \sqrt{1 + (\partial_x \eta_1)^2}\, \nabla \varphi_1 \cdot \boldsymbol{n}_1|_{y=h_1+\eta_1} \end{pmatrix}. \tag{2.13}$$

In the above formulae, $\boldsymbol{n}$ and $\boldsymbol{n}_1$ denote the upwards-pointing unit normal vectors to the interface and surface. In terms of $(\eta, \xi, \eta_1, \xi_1)$, the Hamiltonian is rewritten as

$$\begin{aligned} H = \frac{1}{2} \int \begin{pmatrix} \xi \\ \xi_1 \end{pmatrix}^{\mathrm{T}} \begin{pmatrix} G_{11} B^{-1} G & -G B^{-1} G_{12} \\ -G_{21} B^{-1} G & \dfrac{1}{\rho_1} G_{22} - \dfrac{\rho}{\rho_1} G_{21} B^{-1} G_{12} \end{pmatrix} \begin{pmatrix} \xi \\ \xi_1 \end{pmatrix} \mathrm{d}x \\ + \frac{1}{2} \int g(\rho - \rho_1) \eta^2 \, \mathrm{d}x + \frac{1}{2} \int g \rho_1 [(h_1 + \eta_1)^2 - h_1^2] \, \mathrm{d}x, \end{aligned} \tag{2.14}$$

where $B = \rho G_{11} + \rho_1 G$.

Given their analyticity properties (Craig, Schanz & Sulem 1997), the Dirichlet–Neumann operators (2.12) and (2.13) can be written as convergent Taylor series in $(\eta, \eta_1)$, and each term in these series can be determined recursively. For the sake of completeness, we give the first terms of their Taylor series expansion in appendix A. These series expansions, given with explicit dependence on $(\eta, \eta_1)$, play a central role in the perturbation calculations of this paper.

### 2.3. *Linear analysis and normal mode decomposition*

We briefly recall the linearized equations around a two-layer fluid configuration at rest, since we will later perform a perturbation analysis in this configuration. They are obtained by truncating the Taylor expansion of the Hamiltonian at quadratic order in the variables. Using the operator notation $D = -\mathrm{i}\partial_x$, the quadratic part of the Hamiltonian is given by

$$\begin{aligned} H^{(2)} = \frac{1}{2} \int \xi \frac{D \tanh(hD) \coth(h_1 D)}{\rho \coth(h_1 D) + \rho_1 \tanh(hD)} \xi + 2\xi \frac{D \tanh(hD) \operatorname{csch}(h_1 D)}{\rho \coth(h_1 D) + \rho_1 \tanh(hD)} \xi_1 \\ + \xi_1 \frac{D(\coth(h_1 D) \tanh(hD) + \rho/\rho_1)}{\rho \coth(h_1 D) + \rho_1 \tanh(hD)} \xi_1 + g(\rho - \rho_1) \eta^2 + g \rho_1 \eta_1^2 \, \mathrm{d}x. \end{aligned} \tag{2.15}$$

In order to simplify $H^{(2)}$, we make two scaling canonical transformations. First, a rescaling of the dependent variables

$$\begin{pmatrix} \eta' \\ \xi' \\ \eta_1' \\ \xi_1' \end{pmatrix} = \begin{pmatrix} \sqrt{g(\rho - \rho_1)} & 0 & 0 & 0 \\ 0 & \dfrac{1}{\sqrt{g(\rho - \rho_1)}} & 0 & 0 \\ 0 & 0 & \sqrt{g \rho_1} & 0 \\ 0 & 0 & 0 & \dfrac{1}{\sqrt{g \rho_1}} \end{pmatrix} \begin{pmatrix} \eta \\ \xi \\ \eta_1 \\ \xi_1 \end{pmatrix} \tag{2.16}$$

has the effect of replacing the two last terms of $H^{(2)}$ by $\eta'^2 + \eta_1'^2$. We then diagonalize the kinetic energy in the expression of $H^{(2)}$ by performing the rotation

$$\begin{pmatrix} \mu \\ \zeta \\ \mu_1 \\ \zeta_1 \end{pmatrix} = \begin{pmatrix} a^- & 0 & b^- & 0 \\ 0 & a^- & 0 & b^- \\ a^+ & 0 & b^+ & 0 \\ 0 & a^+ & 0 & b^+ \end{pmatrix} \begin{pmatrix} \eta' \\ \xi' \\ \eta_1' \\ \xi_1' \end{pmatrix}, \tag{2.17}$$

where

$$a^{\pm}(D) = \left(2 + \frac{\theta^2}{2} \pm \frac{\theta}{2}\sqrt{4+\theta^2}\right)^{-1/2}, \tag{2.18}$$

$$b^{\pm}(D) = \frac{1}{2}\left(\theta \pm \sqrt{4+\theta^2}\right)\left(2 + \frac{\theta^2}{2} \pm \frac{\theta}{2}\sqrt{4+\theta^2}\right)^{-1/2}, \tag{2.19}$$

$$\theta(D) = \frac{C(D) - A(D)}{B(D)}, \tag{2.20}$$

and where the Fourier multiplier coefficients $A(D)$, $B(D)$ and $C(D)$ are defined by

$$A(D) = \frac{g(\rho - \rho_1)D\tanh(hD)\coth(h_1D)}{\rho\coth(h_1D) + \rho_1\tanh(hD)}, \tag{2.21a}$$

$$B(D) = \frac{g\sqrt{\rho_1(\rho-\rho_1)}D\tanh(hD)\,\mathrm{csch}(h_1D)}{\rho\coth(h_1D) + \rho_1\tanh(hD)}, \tag{2.21b}$$

$$C(D) = \frac{g\rho_1 D(\coth(h_1D)\tanh(hD) + \rho/\rho_1)}{\rho\coth(h_1D) + \rho_1\tanh(hD)}. \tag{2.21c}$$

As a result, the quadratic part of the Hamiltonian takes the simpler form

$$H^{(2)} = \frac{1}{2}\int (\zeta\omega^2(D)\zeta + \mu^2) + (\zeta_1\omega_1^2(D)\zeta_1 + \mu_1^2)\,\mathrm{d}x, \tag{2.22}$$

where $(\omega^2, \omega_1^2)$ are the two roots of the quadratic equation defining the dispersion relation of the problem. The degrees of freedom described by $(\mu, \zeta)$ represent the 'internal' modes, while those given by $(\mu_1, \zeta_1)$ are the 'free-surface' modes, whose linear dispersion relations are respectively

$$\omega^2(k) = \tfrac{1}{2}\left(A(k) + C(k) - \sqrt{(A(k)-C(k))^2 + 4B^2(k)}\right), \tag{2.23a}$$

$$\omega_1^2(k) = \tfrac{1}{2}\left(A(k) + C(k) + \sqrt{(A(k)-C(k))^2 + 4B^2(k)}\right). \tag{2.23b}$$

These normal modes are linear combinations of the interfacial and surface variables $(\eta, \xi)$ and $(\eta_1, \xi_1)$, respectively. In the limit $k \to \infty$ (short wavelengths), the normal internal (respectively, free-surface) modes tend to coincide with the original internal (respectively, free-surface) modes.

## 3. Derivation of model equations

### 3.1. *Long-wave scaling and modulational ansatz*

The next transformation introduces the long-wave scaling on the internal modes,

$$\mu(x,t) = \varepsilon^2\widetilde{\mu}(X,t), \quad \zeta(x,t) = \varepsilon\widetilde{\zeta}(X,t), \tag{3.1}$$

where $\varepsilon^2 \sim (h/\lambda)^2 \sim a/h \ll 1$ (with $a$ and $\lambda$ being the typical internal wave amplitude and wavelength, respectively) and $X = \varepsilon x$ is a long spatial scale. In addition, one poses the ansatz of quasi-monochromatic modulated waves, adjusted by an additional symplectic transformation on the free-surface modes,

$$\mu_1(x,t) = \frac{\varepsilon_1}{\sqrt{2}}\omega_1^{1/2}(D)(v_1(X,t)\mathrm{e}^{\mathrm{i}k_0 x} + \overline{v}_1(X,t)\mathrm{e}^{-\mathrm{i}k_0 x}) + \varepsilon_1^2\widetilde{\mu}_1(X,t), \quad \widetilde{\mu}_1 = P_0\mu_1, \tag{3.2a}$$

$$\zeta_1(x,t) = \frac{\varepsilon_1}{\sqrt{2}\mathrm{i}}\omega_1^{-1/2}(D)(v_1(X,t)\mathrm{e}^{\mathrm{i}k_0 x} - \overline{v}_1(X,t)\mathrm{e}^{-\mathrm{i}k_0 x}) + \frac{\varepsilon_1^2}{\varepsilon}\widetilde{\zeta}_1(X,t), \quad \widetilde{\zeta}_1 = P_0\zeta_1, \tag{3.2b}$$

where $\varepsilon_1 \sim k_0 a_1 \ll 1$ (with $a_1$ and $k_0$ being the typical carrier wave amplitude and wavenumber, respectively). The overbar symbol denotes complex conjugation, and $P_0$ is the projection that associates to $\mu_1$ and $\xi_1$ their zeroth-frequency components.

The function $v_1$ represents the complex envelope of the free-surface modes, and $\widetilde{\mu}_1$ and $\widetilde{\xi}_1$ the associated mean fields (Craig, Guyenne & Sulem 2010). The presence of the mean fields is necessary to ensure that the transformation $(\mu_1, \zeta_1) \to (v_1, \overline{v}_1, \widetilde{\mu}_1, \widetilde{\zeta}_1)$ is invertible. Furthermore, we transform the system into a moving coordinate frame by subtracting from the Hamiltonian a multiple of the conserved momentum (or impulse)

$$I = \int (\mu\partial_x\zeta + \mu_1\partial_x\zeta_1)\,\mathrm{d}x. \tag{3.3}$$

An expansion of the modified Hamiltonian $H - cI$ (where $c$ is the speed of the moving frame) is obtained by inserting these canonical transformations in (2.14), and expanding in powers of $\varepsilon$ and $\varepsilon_1$,

$$\begin{aligned} H - cI = \int & \frac{\varepsilon_1^2}{\varepsilon}(\omega_1(k_0) - ck_0)\,|v_1|^2 + \frac{1}{2}\varepsilon_1^2(\omega_1'(k_0) - c)(\overline{v}_1 D_X v_1 + v_1\overline{D_X v_1}) \\ & + \frac{1}{4}\varepsilon^3\omega^2\,(0)''\left[\frac{2\widetilde{\mu}^2}{\omega^2\,(0)''}\left(1 - \frac{2c^2}{\omega^2\,(0)''}\right) - \left(D_X\widetilde{\zeta} + \frac{2\mathrm{i}c\widetilde{\mu}}{\omega^2\,(0)''}\right)^2\right] \\ & + \varepsilon^5\left[\frac{1}{48}\omega^2\,(0)''''\,(D_X^2\widetilde{\zeta})^2 + \frac{1}{2}\kappa\widetilde{\mu}\,(D_X\widetilde{\zeta})^2\right] \\ & + \frac{1}{2}\varepsilon\varepsilon_1^2\omega_1''(k_0)\overline{v}_1 D_X^2 v_1 - \frac{1}{4}\frac{\varepsilon_1^4}{\varepsilon}\omega_1^2\,(0)''\,(D_X\widetilde{\zeta}_1)^2 + \frac{1}{2}\frac{\varepsilon_1^4}{\varepsilon}\widetilde{\mu}_1^2 \\ & + \varepsilon\varepsilon_1^2(\kappa_1\widetilde{\mu} + \mathrm{i}\kappa_2 D_X\widetilde{\zeta})\,|v_1|^2 + \frac{\varepsilon_1^4}{\varepsilon}(\kappa_3\widetilde{\mu}_1 + \mathrm{i}\kappa_4 D_X\widetilde{\zeta}_1)\,|v_1|^2 \\ & + \frac{\varepsilon_1^4}{\varepsilon}\kappa_5\,|v_1|^4 - \mathrm{i}c\frac{\varepsilon_1^4}{\varepsilon}\widetilde{\mu}_1 D_X\widetilde{\zeta}_1\,\mathrm{d}X + \text{higher} - \text{order terms}. \end{aligned} \tag{3.4}$$

The notation $f'$ stands for differentiation with respect to the argument of $f$. The scale separation lemmas in Craig *et al.* (2005) imply that fast oscillations in $x$ homogenize to zero and thus do not contribute to the effective Hamiltonian.

### 3.2. *Resonance condition*

Close examination of (3.4) reveals that the choice of speed of the moving frame

$$c^2 = c_0^2 = \frac{\omega^2\,(0)''}{2} = \frac{g}{2}\left(h + h_1 - \sqrt{(h - h_1)^2 + 4\frac{\rho_1}{\rho}hh_1}\right), \tag{3.5}$$

has the result that the third term in (3.4) simplifies, and the resulting Hamiltonian describes a long-wave scaling regime for the evolution of the interface. Given this choice of regime, the carrier wavenumber $k_0$ for the free-surface mode satisfies

$$\omega_1'(k_0) = c_0. \tag{3.6}$$

This condition is interpreted as the resonant interaction between the long internal modes and the short free-surface modes, which occurs when the phase velocity $c_0$ of the former coincides with the group velocity $\omega_1'(k_0)$ of the latter (Lewis *et al.* 1974). There is always a wavenumber $k_0$ satisfying the resonance condition (3.6), and thus a free-surface mode travelling at the same linear speed as the long-wave internal mode. The condition (3.6) simplifies further the expression of the Hamiltonian by making its second term vanish, and (3.4) now takes the form

$$\begin{aligned} H - c_0 I = \int & \frac{\varepsilon_1^2}{\varepsilon}(\omega_1(k_0) - c_0 k_0)\,|v_1|^2 - \frac{1}{2}\varepsilon^3\left(c_0 D_X\widetilde{\zeta} + \mathrm{i}\widetilde{\mu}\right)^2 \\ & + \varepsilon^5\left[\frac{1}{48}\omega^2\,(0)''''\left(D_X^2\widetilde{\zeta}\right)^2 + \frac{1}{2}\kappa\widetilde{\mu}\left(D_X\widetilde{\zeta}\right)^2\right] \\ & + \frac{1}{2}\varepsilon\varepsilon_1^2\omega_1''(k_0)\overline{v}_1 D_X^2 v_1 - \frac{1}{4}\frac{\varepsilon_1^4}{\varepsilon}\omega_1^2\,(0)''\left(D_X\widetilde{\zeta}_1\right)^2 + \frac{1}{2}\frac{\varepsilon_1^4}{\varepsilon}\widetilde{\mu}_1^2 \\ & + \varepsilon\varepsilon_1^2(\kappa_1\widetilde{\mu} + \mathrm{i}\kappa_2 D_X\widetilde{\zeta})\,|v_1|^2 + \frac{\varepsilon_1^4}{\varepsilon}(\kappa_3\widetilde{\mu}_1 + \mathrm{i}\kappa_4 D_X\widetilde{\zeta}_1)\,|v_1|^2 \\ & + \frac{\varepsilon_1^4}{\varepsilon}\kappa_5\,|v_1|^4 - \mathrm{i}c_0\frac{\varepsilon_1^4}{\varepsilon}\widetilde{\mu}_1 D_X\widetilde{\zeta}_1\,\mathrm{d}X + \text{higher}-\text{order terms}. \end{aligned} \tag{3.7}$$

### 3.3. *Regime of small-amplitude free-surface modes*

We assume that the free-surface modes are of smaller amplitude than the internal modes, which is expressed by the choice $\varepsilon_1 = \varepsilon^{2+\gamma}$ $(0 < \gamma \leqslant 1/2)$. Noting that the generalized wave action

$$M = \int |v_1|^2\,\mathrm{d}X \tag{3.8}$$

is also a conserved quantity of the system at this order of approximation, we can adjust the phase of solutions by adding a multiple of the wave action, further reducing the Hamiltonian to

$$\begin{aligned} \widehat{H} &= H - c_0 I - \varepsilon^{3+2\gamma}(\omega_1(k_0) - c_0 k_0)M, \\ &= \int \frac{1}{2}\varepsilon^3\left(\widetilde{\mu} - c_0\widetilde{u}\right)^2 + \varepsilon^5\left[\frac{1}{48}\omega^2\,(0)''''\left(\partial_X\widetilde{u}\right)^2 - \frac{1}{2}\kappa\widetilde{\mu}\,\widetilde{u}^2\right] \\ &\quad + \varepsilon^{5+2\gamma}\left[\frac{1}{2}\omega_1''(k_0)\,|\partial_X v_1|^2 + (\kappa_1\widetilde{\mu} + \kappa_2\widetilde{u})\,|v_1|^2\right] \\ &\quad + \varepsilon^{7+4\gamma}\left[\frac{1}{4}\omega_1^2\,(0)''\left(\partial_X\widetilde{\zeta}_1\right)^2 + \frac{1}{2}\widetilde{\mu}_1^2 + (\kappa_3\widetilde{\mu}_1 + \kappa_4\partial_X\widetilde{\zeta}_1)\,|v_1|^2\right. \\ &\quad \left. + \kappa_5\,|v_1|^4 - c_0\widetilde{\mu}_1\partial_X\widetilde{\zeta}_1\right]\mathrm{d}X + o(\varepsilon^9), \end{aligned} \tag{3.9}$$

where $\widetilde{u} = \partial_X\widetilde{\zeta}$ represents an internal shear velocity. The conservation of $M$ (and the fact that we may subtract it from $H$ without changing the evolution) reflects the

fact that our approximation in this regime is phase-invariant. Therefore, $\widehat{H}$ describes the essential dynamics of the system at the order of approximation that is being considered.

### 3.4. *Coupled KdV–Schrödinger system*

The last step in our derivation is a transformation to characteristic coordinates

$$\begin{pmatrix} r \\ s \end{pmatrix} = \begin{pmatrix} \dfrac{1}{\sqrt{2c_0}} & \sqrt{\dfrac{c_0}{2}} \\ \dfrac{1}{\sqrt{2c_0}} & -\sqrt{\dfrac{c_0}{2}} \end{pmatrix} \begin{pmatrix} \widetilde{\mu} \\ \widetilde{u} \end{pmatrix}, \tag{3.10}$$

where $r(X,t)$ and $s(X,t)$ are the internal components that are principally right-moving and left-moving, respectively. We look primarily at internal modes propagating to the right, which is accomplished by an additional scaling $s = \varepsilon^2 s_0$ with $s_0 = O(1)$. Eliminating higher-order contributions, this leads to the reduced Hamiltonian of four terms

$$\begin{aligned} \widehat{H} = \varepsilon^5 \int & \frac{\omega^2(0)''''}{96c_0}\left[(\partial_X r)^2 - \frac{\kappa}{4\sqrt{2c_0}} r^3\right] \\ & + \varepsilon^{5+2\gamma}\left[\frac{1}{2}\omega_1''(k_0)\,|\partial_X v_1|^2 + \widetilde{\kappa}_1 r\,|v_1|^2\right] \mathrm{d}X, \end{aligned} \tag{3.11}$$

where

$$\widetilde{\kappa}_1 = \sqrt{\frac{c_0}{2}}\left(\kappa_1 + \frac{\kappa_2}{c_0}\right), \quad \widetilde{\kappa}_2 = \sqrt{\frac{c_0}{2}}\left(\kappa_1 - \frac{\kappa_2}{c_0}\right). \tag{3.12}$$

Setting $\tau = \varepsilon^3 t$ and using (3.11) and the accompanying change of symplectic form, the evolution equation for $r$ reads

$$\begin{aligned} \partial_\tau r &= -\varepsilon^2 \partial_X \delta_r \widehat{H}, \\ &= \frac{\omega^2(0)''''}{48c_0}\partial_X^3 r + \frac{3\kappa}{2\sqrt{2c_0}} r\partial_X r - \varepsilon^{2\gamma}\widetilde{\kappa}_1 \partial_X |v_1|^2, \end{aligned} \tag{3.13}$$

while by setting $\tau_1 = \varepsilon^2 t$, the equation for $v_1$ takes the form

$$\begin{aligned} \partial_{\tau_1} v_1 &= -\mathrm{i}\varepsilon^{-3-2\gamma}\delta_{\overline{v}_1}\widehat{H}, \\ &= \mathrm{i}[\tfrac{1}{2}\omega_1''(k_0)\partial_X^2 v_1 - \widetilde{\kappa}_1 r v_1], \end{aligned} \tag{3.14}$$

the linear Schrödinger equation for the free-surface modes, with a time-dependent potential proportional to $r$. Finally, at lowest order, equation (3.13) reduces to a KdV equation,

$$\partial_\tau r = \frac{\omega^2(0)''''}{48c_0}\partial_X^3 r + \frac{3\kappa}{2\sqrt{2c_0}} r\partial_X r, \tag{3.15}$$

for the internal modes.

A version of the derivation of these model equations is presented in Craig, Guyenne & Sulem (2011), to which the reader can refer for further details of this derivation. However, this reference does not provide the explicit expressions of various interaction coefficients $\kappa_j$ that appear in the evolution equations and in their Hamiltonian. These

interaction terms are given in appendix B, while their significance is discussed in the next section.

## 4. Analysis of the KdV–Schrödinger system and interpretation

General motions of this free interface–surface configuration, in the regime of long-wave internal modes in resonance with the free surface, are described by the coupled system (3.14) and (3.15). We note that the time scales for the KdV equation and the Schrödinger equation are different, $\tau = \varepsilon^3 t$ (with $t$ being the actual physical time) and $\tau_1 = \varepsilon^2 t$. The component $r$ is closely related to the internal wave, while $v_1$ is the modulated amplitude related to the fast oscillations of the surface wave. In the regime of interest ($\varepsilon \ll 1$, $0 < \gamma \leqslant 1/2$), the nonlinear coupling terms in the KdV equation (3.13) are essentially negligible, and the coupling with the KdV equation appears through a linear operator given by the potential. This is as one expects from physical observations, and is the situation on which we will focus. If $\gamma = 0$, meaning that the amplitudes of the internal and surface waves are comparable, there are other coupling terms that appear as forcing terms in the KdV equation, and the dynamics are more complex.

In the following, we construct solutions to the above system (3.14) and (3.15), which are, as a consequence, approximate solutions to the original problem. Our goal is to exhibit solutions that have many of the features of the waves observed in the context of *in situ* measurements and in satellite photographs.

### 4.1. *Dependence of coefficients on density ratio and relative depth*

The leading-order approximation to system (2.1)–(2.7) in the asymptotic regime of interest is (3.14) and (3.15), which are rewritten as

$$\partial_\tau r + a_1 r \partial_X r + a_2 \partial_X^3 r = 0, \tag{4.1}$$

$$\partial_{\tau_1} v_1 = \mathrm{i}[\tfrac{1}{2}\omega_1''(k_0)\partial_X^2 v_1 + a_3 r(X, \varepsilon\tau_1) v_1], \tag{4.2}$$

with coefficients being given by

$$a_1 = -\sqrt{\frac{c_0}{2}}\frac{3\kappa}{2c_0}, \quad a_2 = -\frac{\omega^2(0)''''}{48c_0}, \quad a_3 = -\widetilde{\kappa}_1. \tag{4.3}$$

These can be explicitly expressed in terms of two free parameters, the relative density $\rho_1/\rho$ and the relative depth $h_1/h$ of the two fluids, which are given in appendix B.

The single-soliton solution of the KdV equation is given by

$$r(X, \tau) = \frac{3a_2 u_0}{a_1}\mathrm{sech}^2\left[\frac{\sqrt{u_0}}{2}(X - a_2 u_0 \tau)\right]. \tag{4.4}$$

Depending on the sign of $a_1/a_2$, the single-soliton solution (4.4) of the KdV equation (4.1) is a wave of depression or elevation. This expression is similar to that derived by Peters & Stoker (1960).

In realistic conditions, the ratio $\rho_1/\rho$ is close to 1 (Helfrich & Melville 2006). Taking this into account, we evaluate (numerically) the coefficients as functions of $h_1/h$. Figure 1 shows that $a_2$ (solid line) is always positive while $a_1$ (dashed line) changes sign when $h_1/h$ passes a particular value. Indeed, it is clear that $a_1 < 0$ if $h_1/h$ is small and $a_1 > 0$ otherwise, which implies that soliton-like profiles of the interface mode are waves of depression in the regime of interest.

We now turn to the linear Schrödinger equation (4.2). For $\rho_1/\rho$ and $h_1/h$ given, the speed $c_0$ is defined by (3.5), from which the wavenumber $k_0$ is uniquely determined

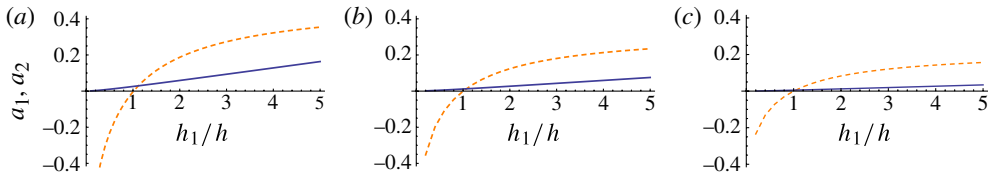


FIGURE 1. (Colour online) Parameters $a_1$ (dashed line) and $a_2$ (solid line) as functions of depth ratio $h_1/h$. The density ratio is $\rho_1/\rho = 0.95$ (*a*), 0.99 (*b*) and 0.998 (*c*). This implies that, for $h_1/h \leqslant C \sim O(1)$, soliton solutions (4.4) take the form of a depression at the interface.

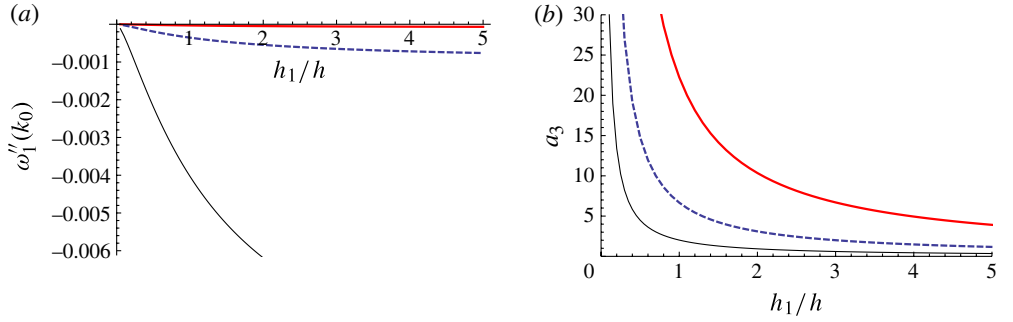


FIGURE 2. (Colour online) Dispersion coefficient $\omega_1''(k_0)$ (*a*) and parameter $a_3$ (*b*) as functions of $h_1/h$ for $\rho_1/\rho = 0.95$ (thin line), 0.99 (dashed line) and 0.998 (thick line).

through the resonance condition (3.6) as shown in Craig *et al.* (2011). We see in figure 2 that, for $\rho_1/\rho$ close to 1, the coupling constant $a_3$ is positive while the coefficient of dispersion $\omega_1''(k_0)$ is always negative. As $h_1/h$ decreases, $\omega_1''(k_0)$ tends to zero while $a_3$ is of order $O(1)$ or larger.

We now confine our considerations to the case in which the internal mode $r(X, \tau)$ is given by the single-soliton solution (4.4), for which (4.2) further simplifies. Performing the change of variables

$$v_1(X, \tau_1) = \mathrm{e}^{\mathrm{i}(p_1 y + p_2 z)} w(y, z), \tag{4.5}$$

where

$$y = X - \varepsilon a_2 u_0 \tau_1, \quad z = a_3 \tau_1, \quad p_1 = \frac{\varepsilon a_2 u_0}{\omega_1''(k_0)}, \quad p_2 = \frac{(\varepsilon a_2 u_0)^2}{2 a_3 \omega_1''(k_0)}, \tag{4.6}$$

and denoting

$$\frac{\omega_1''(k_0)}{2a_3} = -\delta^2, \tag{4.7}$$

the Schrödinger equation reduces to

$$-\mathrm{i}\partial_z w = -\delta^2 \partial_y^2 w + r w. \tag{4.8}$$

The parameter $\delta^2$ is displayed in figure 3 as a function of $h_1/h$ for $\rho_1/\rho = 0.95$, 0.99 and 0.998.

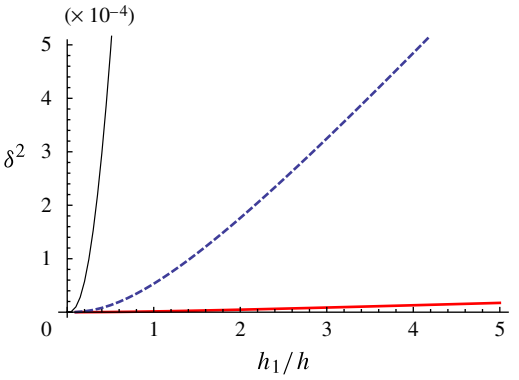


FIGURE 3. (Colour online) Parameter $\delta^2$ in (4.8) as a function of $h_1/h$ for $\rho_1/\rho = 0.95$ (thin line), 0.99 (dashed line) and 0.998 (thick line).

The general solution of (4.8) has a spectral decomposition in the form of a linear superposition of solutions

$$w(y, z) = \int e^{i\lambda z} u(y, \lambda)\, d\mu(\lambda), \tag{4.9}$$

where $u(y, \lambda)$ satisfies

$$-\delta^2 \partial_y^2 u + ru = \lambda u. \tag{4.10}$$

The spectrum of the operator $-\delta^2\partial_y^2 + r$ is composed of a finite number of negative eigenvalues $\lambda_0 < \lambda_1 < \cdots < \lambda_N < 0$, which are associated with localized bound states, along with the continuous spectrum $\lambda > 0$. The absorption spectrum of the bound states and the scattering characteristics of the continuous spectrum serve to describe the evolution properties of a general solution to (4.8).

### 4.2. *Bound states in the regime* $h_1/h < 1$, $\rho - \rho_1 \ll \rho + \rho_1$

In this regime typical of, for example, coastal seas (Osborne & Burch 1980; Bakhanov & Ostrovsky 2002; Bourgault & Kelley 2003), figure 3 illustrates that $\delta \ll 1$, and since $r < 0$ (figure 1), the internal soliton plays the role of a potential well. This situation is analogous to the semi-classical limit in quantum mechanics. In the semi-classical regime, the number of negative eigenvalues $\{\lambda_j\}_{j=0,\ldots,N}$ is large but finite, $N \sim \delta^{-1}$, with corresponding localized bound states $\{\psi_j(y)\}_{j=0,\ldots,N}$, which can be characterized by their number of zeros.

A numerical calculation in which $\rho_1/\rho = 0.997$, $h_1/h = 0.2$ and $r$ is specified by (4.4) with $\|r\|_{L^\infty} = 0.5$ gives rise to $N = 547$ bound states, with the smallest eigenvalue being $\lambda_0 = -0.4959$ (figure 4). We use the very efficient and accurate Fourier grid Hamiltonian method of Marston & Balint-Kurti (1989), which computes derivatives in Fourier space using the fast Fourier transform, while the potential is evaluated at grid points in physical space. The bound states $\psi_j$ and corresponding energies $\lambda_j$ are found by computing the eigenfunctions and eigenvalues of the Hamiltonian bra-ket matrix associated with (4.10), for which 8192 grid points are typically used in the computations.

Figures 5 and 6 show the internal soliton and its surface signature in terms of the physical variables $(\eta, \eta_1)$ for the choice of a ground bound state at the free surface,

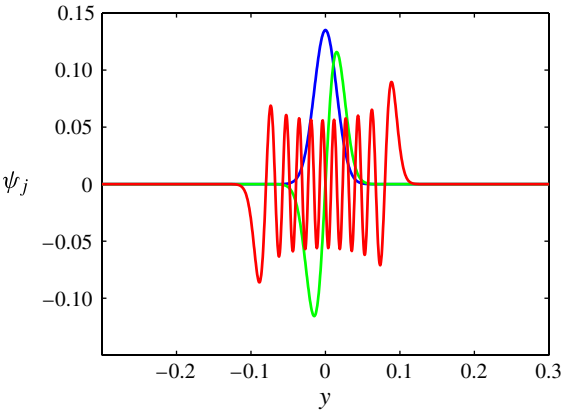


FIGURE 4. (Colour online) Superimposed image of three bound states $\psi_j$ (ground state, $j = 2$ and $j = 20$) for a soliton potential (4.4) with parameters $\rho_1/\rho = 0.997$, $h_1/h = 0.2$ and $\|r\|_{L^\infty} = 0.5$.

in oceanic conditions corresponding to the Andaman Sea and off the Oregon coast, respectively. Typical parameters for the Andaman Sea are $\rho_1/\rho = 0.997$, $h_1/h = 0.266$ and $\varepsilon^2 \sim a/h = 0.069$, as given by Osborne & Burch (1980), who reported $h_1 = 230$ m, $h = 863$ m and internal waves of amplitude $a \sim 60$ m (see also Evans & Ford 1996). Typical parameters for COPE data measured off the Oregon coast are $\rho_1/\rho = 0.998$, $h_1/h = 0.035$ and $\varepsilon^2 \sim a/h = 0.192$, as given by Bakhanov & Ostrovsky (2002), who reported $h_1 = 5$ m, $h = 143$ m and internal waves of amplitude $a \sim 27.5$ m. The corresponding values of $k_0$ (i.e. the surface carrier wavenumber) are computed from the resonance condition (3.6).

Both figures clearly illustrate the disparity in length scales between the internal and surface waves as well as the localized shape of the surface modulation, which are characteristic features of the rip phenomenon as depicted, for example, in figures 3 of Osborne & Burch (1980) and of Alpers (1985). We note in particular that the value $k_0 h = 3696.2$ for figure 6 implies that the surface wavelength is $l_0 = 2\pi/k_0 = 24$ cm, which is consistent with observations of surface ripples of wavelengths ∼20 cm as discussed in Bakhanov & Ostrovsky (2002).

We next estimate the absorption of energy into the bound states as the internal soliton propagates into an ambient sea state. This energy trapping at the free surface gives an explanation for the rip phenomenon associated with the surface signature of internal waves. The initial state of the sea-surface modulation is described through $w(y, 0)$, after the sequence of transformations given in §§ 3.1 and 4.1. The Fourier transform decomposition of $w(y, 0)$ projects onto the bound states of the spectral decomposition of the Schrödinger operator (4.10) through the expression

$$\langle w(y, 0), \psi_j(y) \rangle = \frac{1}{\sqrt{2\pi}} \int_{-\infty}^{\infty} S_j(k) \widehat{w}(k, 0)\, \mathrm{d}k, \tag{4.11}$$

where

$$S_j(k) = \frac{1}{\sqrt{2\pi}} \int_{-\infty}^{\infty} \mathrm{e}^{-\mathrm{i}ky} \psi_j(y)\, \mathrm{d}y. \tag{4.12}$$

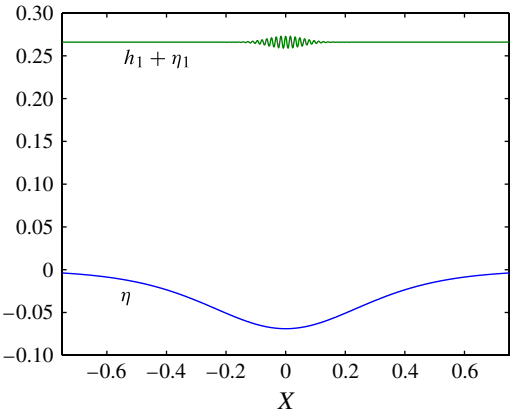


FIGURE 5. (Colour online) Internal and surface waves in the physical variables $(\eta, \eta_1)$ for $\rho_1/\rho = 0.997$, $h_1/h = 0.266$, $a/h = 0.069$ and $k_0 h = 396.4$ (Andaman Sea). The reference length scale is $h = 1$ in dimensionless units. For clarity, the surface wave amplitude is magnified in order to show details of the rip region.

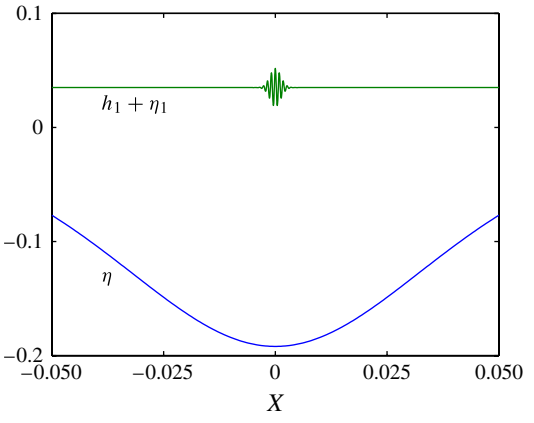


FIGURE 6. (Colour online) Internal and surface waves in the physical variables $(\eta, \eta_1)$ for $\rho_1/\rho = 0.998$, $h_1/h = 0.035$, $a/h = 0.192$ and $k_0 h = 3696.2$ (off the Oregon coast). The reference length scale is $h = 1$ in dimensionless units. For clarity, the surface wave amplitude is magnified in order to show details of the rip region.

The latter represents the Fourier absorption profile of the bound state $\psi_j$. The following proposition indicates that this absorption spectrum is non-trivial.

PROPOSITION 4.1. *In the limit* $\delta \to 0$, *for wavenumbers* $k$ *such that* $0 < |k| < \sqrt{\lambda_j - r(0)}/\delta$, *there is a lower bound*

$$C\left(\frac{\delta}{j}\right)^{1/4} \leqslant S_j(k) \tag{4.13}$$

*on the amplitude of the absorption spectral density.*

***Proof.*** In the limit $\delta \to 0$, the Wentzel–Kramers–Brillouin (WKB) method describes the form of the eigenvalues $r(0) < \lambda_j < 0$ and the quantization condition determining these eigenvalues,

$$\frac{1}{\delta}\int_{-y_j}^{y_j} [\lambda_j - r(y)]^{1/2}\, \mathrm{d}y = \left(j + \frac{1}{2}\right)\pi + O(\delta), \tag{4.14}$$

where $\pm y_j = \pm y(\lambda_j)$ are the two turning points of $r(y) - \lambda_j$. Because of the asymptotic behaviour

$$\int_{-y_j}^{y_j} [\lambda_j - r(y)]^{1/2}\, \mathrm{d}y \sim \frac{4}{3} r'(y_j)^{1/2} y_j^{3/2} \sim y_j^2, \tag{4.15}$$

the quantization condition implies that

$$y_j = O([(j + \tfrac{1}{2})\delta]^{1/2}). \tag{4.16}$$

In the oscillatory regions $-y_j < y < y_j$, the bound states $\psi_j$ have the asymptotic behaviour

$$\psi_j(y) \sim C_j\, [\lambda_j - r(y)]^{-1/4} \sin\left[\frac{1}{\delta}\Phi_j(y) + \frac{\pi}{4}\right], \tag{4.17}$$

with the phase

$$\Phi_j(y) = \int_{y}^{y_j} [\lambda_j - r(y')]^{1/2}\, \mathrm{d}y'. \tag{4.18}$$

In the regions $|y| > y_j$, eigenfunctions decay exponentially. Denoting $k = k'/\delta$, we approximate $S_j(k)$ by

$$S_j(k) \sim C_j \int_{-y_j}^{y_j} [\lambda_j - r(y)]^{-1/4} \sin\left[\frac{1}{\delta}\Phi_j(y) + \frac{\pi}{4}\right] \mathrm{e}^{-\mathrm{i}ky}\, \mathrm{d}y. \tag{4.19}$$

For $0 < |k'| < \sqrt{\lambda_j - r(0)}$, there are two stationary phase points $\pm y_j(k)$ defined as the roots of $k' = \pm\sqrt{\lambda_j - r(y)}$, where $0 < |y_j(k)| < y_j$. Using the method of stationary phase, we find

$$S_j(k) \sim C_j \left[\frac{\delta}{r'(y_j(k))}\right]^{1/2}. \tag{4.20}$$

Finally, we evaluate the normalizing constant $C_j$ according to

$$1 = \|\psi_j\|_{L^2}^2 \sim |C_j|^2 \int_{-y_j}^{y_j} [\lambda_j - r(y)]^{-1/2} \sin^2\left[\frac{1}{\delta}\Phi_j(y) + \frac{\pi}{4}\right] \mathrm{d}y, \tag{4.21}$$

which, by the method of stationary phase again, yields $C_j = O(1)$. □

The significance of this analysis is twofold. First of all, the statement (4.16) about the turning points of the $j$th bound state is an estimate on the size of its oscillatory region, from which we conclude that the active width of the bound state is of the order of $O([(j + \frac{1}{2})\delta]^{1/2})$, and furthermore that it is principally located in the middle of the potential well. This estimate, which is dependent on $\delta \ll 1$, is a measure of the narrowness of the rip region. Secondly, the absorption spectral density function $S_j(k)$ represents the coupling coefficient between the component of the surface wave field

at wavenumber $k$ and the $j$th bound state. The lower bound of this proposition gives a lower estimate of the transfer of energy from the surface wave field to this bound state. Indeed, given an ambient background state $B(x)$ of relatively broad spectrum, its contribution to any particular bound state $\psi_j$ is proportional to the total energy, and is essentially

$$|\langle \widehat{B}, S_j \rangle| \geqslant C \left(\frac{\delta}{j}\right)^{1/4} \left( \int_{-\infty}^{\infty} |\widehat{B}|^2 \, \mathrm{d}k \right)^{1/2}. \tag{4.22}$$

The total energy captured by the passing potential well is given by

$$\sum_{j=0}^{N} |B_j|^2 = \sum_{j=0}^{N} |\langle \widehat{B}, S_j \rangle|^2 . \tag{4.23}$$

Since $N \sim O(\delta^{-1})$, this has a lower bound

$$C\delta^{1/2} \sum_{j=0}^{N} \frac{1}{j^{1/2}} \|B\|_{L^2}^2 = \frac{1}{2} C\delta^{1/2} N^{1/2} \|B\|_{L^2}^2 = O(1) \|B\|_{L^2}^2, \tag{4.24}$$

implying that a positive proportion of the ambient sea state is able to be captured by this process.

### 4.3. *Reflection and transmission coefficients in the regime $h_1/h$ small*

We now turn to the continuous spectrum of (4.10), which consists of the whole semi-axis $\lambda > 0$. From the frame of reference of the soliton, the background sea state is incident on the potential well described by $r(y)$, and Fourier components of this sea state are absorbed, reflected or transmitted by it. In the semi-classical regime $\delta \ll 1$, the potential well acts as a barrier, in the sense that, for an interval of wavenumbers $k^2 = \lambda \in [0, \lambda(\delta)]$, the reflection coefficient is dominant for waves incident on the potential, and their transmission coefficient is small. Indeed, our explanation of the 'mill pond' effect is the surface dynamics that result from this phenomenon. Namely, from a stationary reference point on the sea surface, a passing internal soliton absorbs a significant component of the background sea state, while reflecting a further significant component of the wavenumbers $k \in [-\sqrt{\lambda(\delta)}, \sqrt{\lambda(\delta)}]$, essentially sweeping this sea state in front of it, and permitting little radiation to be transmitted through the soliton to the sea surface behind it.

For this purpose, one seeks solutions of (4.10) with $\lambda > 0$ in the continuous spectrum, in the form of plane waves at $\pm\infty$ with

$$u(y) \sim \mathrm{e}^{-\mathrm{i}\sqrt{\lambda} y/\delta} + b\, \mathrm{e}^{\mathrm{i}\sqrt{\lambda} y/\delta} \quad \text{as } y \to +\infty, \tag{4.25a}$$

$$u(y) \sim c\, \mathrm{e}^{-\mathrm{i}\sqrt{\lambda} y/\delta} \quad \text{as } y \to -\infty. \tag{4.25b}$$

The coefficients $b = b(\lambda, \delta)$ and $c = c(\lambda, \delta)$ are respectively the reflection and transmission coefficients.

PROPOSITION 4.2. *In the limit $\delta, \lambda \to 0$ with the condition $\sqrt{\lambda}/\delta \to 0$, the coefficients of reflection and transmission have the asymptotic values $b = -1 + O(\sqrt{\lambda})$ and $c = O(\sqrt{\lambda})$ , respectively.*

***Proof.*** We write expressions for the solution of (4.10) in the three regions $(-\infty, -A]$, $(-A, A)$ and $[A, \infty)$ of the real axis, and conditions on the coefficients $b$ and $c$ will

be obtained by imposing continuity of the solution and its first-order derivative at the matching points $\pm A$.

On the right half-axis $A < y < +\infty$, the solution can be written as

$$u_+(y) = \mathrm{e}^{-\mathrm{i}\sqrt{\lambda}y/\delta} + b\,\mathrm{e}^{\mathrm{i}\sqrt{\lambda}y/\delta} - \frac{1}{\delta\sqrt{\lambda}}\int_y^{+\infty} \sin\left[\frac{\sqrt{\lambda}}{\delta}(y-y')\right] r(y')u_+(y')\,\mathrm{d}y', \quad (4.26)$$

and on the left half-axis $-\infty < y < -A$,

$$u_-(y) = c\,\mathrm{e}^{-\mathrm{i}\sqrt{\lambda}y/\delta} + \frac{1}{\delta\sqrt{\lambda}}\int_{-\infty}^{y} \sin\left[\frac{\sqrt{\lambda}}{\delta}(y-y')\right] r(y')u_-(y')\,\mathrm{d}y'. \quad (4.27)$$

The function $u_+$ (and similarly $u_-$) can be obtained by successive approximations as defined by the sequence

$$u_+^{(0)} = \mathrm{e}^{-\mathrm{i}\sqrt{\lambda}y/\delta} + b\,\mathrm{e}^{\mathrm{i}\sqrt{\lambda}y/\delta}, \quad (4.28a)$$

$$u_+^{(n)} = \mathrm{e}^{-\mathrm{i}\sqrt{\lambda}y/\delta} + b\,\mathrm{e}^{\mathrm{i}\sqrt{\lambda}y/\delta} - \frac{1}{\delta\sqrt{\lambda}}\int_y^{+\infty} \sin\left[\frac{\sqrt{\lambda}}{\delta}(y-y')\right] r(y')u_+^{(n-1)}(y')\,\mathrm{d}y', \quad (4.28b)$$

which is convergent for all $\sqrt{\lambda}/\delta$ with $\mathrm{Im}(\sqrt{\lambda}/\delta) \geqslant 0$ (Chadan *et al.* 1997). In our approximation, we only take two steps in the iterative process,

$$u_+(y) = \mathrm{e}^{-\mathrm{i}\sqrt{\lambda}y/\delta} + b\,\mathrm{e}^{\mathrm{i}\sqrt{\lambda}y/\delta} - \frac{1}{\delta\sqrt{\lambda}}\int_y^{+\infty} \sin\left[\frac{\sqrt{\lambda}}{\delta}(y-y')\right] r(y')(\mathrm{e}^{-\mathrm{i}\sqrt{\lambda}y'/\delta} + b\,\mathrm{e}^{\mathrm{i}\sqrt{\lambda}y'/\delta})\,\mathrm{d}y'. \quad (4.29)$$

Similarly, for $y < -A$,

$$u_-(y) = c\left(\mathrm{e}^{-\mathrm{i}\sqrt{\lambda}y/\delta} + \frac{1}{\delta\sqrt{\lambda}}\int_{-\infty}^{y} \sin\left[\frac{\sqrt{\lambda}}{\delta}(y-y')\right] r(y')\mathrm{e}^{-\mathrm{i}\sqrt{\lambda}y'/\delta}\,\mathrm{d}y'\right). \quad (4.30)$$

In appendix C, we show that this approximation is valid if the cut-off $A$ is chosen large enough. In the intermediate region $-A < y < A$, we use the WKB approximation

$$u_0(y) \sim [\lambda - r(y)]^{-1/4}(\alpha\,\mathrm{e}^{-\mathrm{i}\int_0^y \sqrt{\lambda - r(s)}\,\mathrm{d}s/\delta} + \beta\,\mathrm{e}^{\mathrm{i}\int_0^y \sqrt{\lambda - r(s)}\,\mathrm{d}s/\delta}). \quad (4.31)$$

The continuity of the solution and its first-order derivative at $y = \pm A$ gives four conditions for the four constants $(b, c, \alpha, \beta)$.

Denoting $k = \sqrt{\lambda}/\delta$, the continuity of the solution at $y = +A$ yields

$$\mathrm{e}^{-\mathrm{i}kA} + b\,\mathrm{e}^{\mathrm{i}kA} - \frac{1}{\delta\sqrt{\lambda}}\int_A^{+\infty} \sin[k(A-y)]r(y)(\mathrm{e}^{-\mathrm{i}ky} + b\,\mathrm{e}^{\mathrm{i}ky})\,\mathrm{d}y$$
$$= [\lambda - r(A)]^{-1/4}(\alpha\,\mathrm{e}^{-\mathrm{i}\int_0^A \sqrt{\lambda - r(s)}\,\mathrm{d}s/\delta} + \beta\,\mathrm{e}^{\mathrm{i}\int_0^A \sqrt{\lambda - r(s)}\,\mathrm{d}s/\delta}). \quad (4.32)$$

Rewriting the integral

$$\int_0^A \sqrt{\lambda - r(s)}\,\mathrm{d}s = A\sqrt{\lambda} + J, \quad (4.33)$$

with

$$J = \int_0^A \left[\sqrt{\lambda - r(s)} - \sqrt{\lambda}\right] \mathrm{d}s, \quad (4.34)$$

equation (4.32) becomes

$$b + \mathrm{e}^{-2\mathrm{i}kA} - \frac{1}{2\mathrm{i}\delta\sqrt{\lambda}} \int_A^{+\infty} [\mathrm{e}^{-2\mathrm{i}ky} - \mathrm{e}^{-2\mathrm{i}kA} + b(1 - \mathrm{e}^{-2\mathrm{i}k(A-y)})] r(y)\, \mathrm{d}y$$
$$= [\lambda - r(A)]^{-1/4} (\alpha\, \mathrm{e}^{-\mathrm{i}J/\delta} \mathrm{e}^{-2\mathrm{i}kA} + \beta\, \mathrm{e}^{\mathrm{i}J/\delta}). \tag{4.35}$$

Similarly, the continuity of $u$ at $y = -A$ implies that

$$c \left[ 1 - \frac{1}{2\mathrm{i}\delta\sqrt{\lambda}} \int_{-\infty}^{-A} (1 - \mathrm{e}^{-2\mathrm{i}k(A+y)}) r(y)\, \mathrm{d}y \right]$$
$$= [\lambda - r(A)]^{-1/4} (\alpha\, \mathrm{e}^{\mathrm{i}J/\delta} + \beta\, \mathrm{e}^{-\mathrm{i}J/\delta} \mathrm{e}^{-2\mathrm{i}kA}). \tag{4.36}$$

The two equations coming from the matching of the first-order derivatives at $y = \pm A$ are

$$b - \mathrm{e}^{-2\mathrm{i}kA} - \frac{1}{2\mathrm{i}\delta\sqrt{\lambda}} \int_A^{+\infty} [\mathrm{e}^{-2\mathrm{i}ky} + \mathrm{e}^{-2\mathrm{i}kA} + b(1 + \mathrm{e}^{-2\mathrm{i}k(A-y)})] r(y)\, \mathrm{d}y$$
$$= \alpha \left( \frac{1}{4ik} r'(A) [\lambda - r(A)]^{-5/4} - \frac{1}{\sqrt{\lambda}} [\lambda - r(A)]^{1/4} \right) \mathrm{e}^{-\mathrm{i}J/\delta} \mathrm{e}^{-2\mathrm{i}kA}$$
$$+ \beta \left( \frac{1}{4ik} r'(A) [\lambda - r(A)]^{-5/4} + \frac{1}{\sqrt{\lambda}} [\lambda - r(A)]^{1/4} \right) \mathrm{e}^{\mathrm{i}J/\delta} \tag{4.37}$$

and

$$c \left[ 1 - \frac{1}{2\mathrm{i}\delta\sqrt{\lambda}} \int_{-\infty}^{-A} (1 + \mathrm{e}^{-2\mathrm{i}k(A+y)}) r(y)\, \mathrm{d}y \right]$$
$$= \alpha \left( \frac{1}{4ik} r'(A) [\lambda - r(A)]^{-5/4} + \frac{1}{\sqrt{\lambda}} [\lambda - r(A)]^{1/4} \right) \mathrm{e}^{\mathrm{i}J/\delta}$$
$$+ \beta \left( \frac{1}{4ik} r'(A) [\lambda - r(A)]^{-5/4} - \frac{1}{\sqrt{\lambda}} [\lambda - r(A)]^{1/4} \right) \mathrm{e}^{-\mathrm{i}J/\delta} \mathrm{e}^{-2\mathrm{i}kA}. \tag{4.38}$$

This system is solved in matrix form $\boldsymbol{MX} = \boldsymbol{B}$ for the unknown vector $\boldsymbol{X} = (b, c, \alpha, \beta)^{\mathrm{T}}$, using Maple. The $4 \times 4$ coefficient matrix $\boldsymbol{M}$ and right-hand side vector $\boldsymbol{B}$ are given in appendix D. We then expand the solution for $\lambda$ small and get the conclusion of the proposition. □

We point out here that $k = \sqrt{\lambda}/\delta$ plays the role of sideband wavenumbers since it is associated with solutions of the Schrödinger equation (4.2). Therefore, the limit $k \to 0$ for free-surface modes corresponds to the case of pure monochromatic waves of carrier wavenumber $k_0$ as defined by (3.6).

## 5. Conclusions

This paper addresses the nonlinear interaction of internal waves and free-surface waves in an ocean with two distinct layers. Using a form of Hamiltonian perturbation theory, we show that long internal waves are modelled by the KdV equation (4.1), which then generate a resonant interaction with a modulated surface wave at resonant wavenumber $k_0$. In the regime of relatively calm seas, the surface wave envelope is described by a linear Schrödinger equation (4.2) with potential given by the internal

wave. In the common situation in which $h_1 < h$ and $\rho - \rho_1 \ll \rho + \rho_1$ (small Atwood number), the coefficient of dispersion $\omega_1''(k_0)/(2a_3)$ is very small and solutions of (4.2) propagate in the semi-classical regime. This gives rise to an analogy with semi-classical quantum mechanics, and the phenomenon of radiative absorption. A soliton internal wave solution plays the role of a potential well, which has the capability of absorbing energy into its bound states as the soliton propagates into a regime of a background ambient sea state. The accumulation of energy in the bound states of this potential gives rise to the rip phenomenon. Semi-classical bound states are very well localized, and they are essentially supported near the minimum of the potential well. This fact gives at the same time an explanation of the narrowness of the regions of rip, and at least in the idealized situation of an internal soliton, a description of their location. Secondly, in the semi-classical regime, a potential well acts as an obstacle to transmission, much as a potential barrier does, with the result that surface waves contributing to the ambient sea state at any sideband wavenumbers are almost perfectly reflected. From a fixed reference point on the sea surface, the passage of an internal soliton reflects the waves propagating in front of it, effectively sweeping the surface of waves, and resulting in the observed phenomenon of the mill pond-like calm after its passage.

This description of the phenomenon of surface wave signatures reproduces many of their most important features. This includes the striking narrowness of observed rip regions, which contrasts with the known broadening of internal solitons. It also explains the uniformity of the rip over large lateral distances, which avoids the assumption of a uniform ambient sea state over such large regions. Finally, it gives a linear and conservative explanation of the mill pond effect, again avoiding dependence on wave breaking or on other dissipative mechanisms. The theory gives rise to a prediction that a finer Fourier analysis of observed rip regions will exhibit a dominant wavenumber, namely $k_0$, stemming from the internal–surface mode resonance.

Our analysis has neglected a certain number of points. First of all, an ambient background sea surface with a two-dimensional background sea state should be considered; this however could be treated by our methods using separation of variables. Time-dependent internal waves are a more serious consideration. Our approach permits a transformation to a stationary frame of reference in the case of an internal soliton, but more general internal wave motions lead to the Schrödinger equation with a slowly varying time-dependent potential. A possible future treatment of this situation would be through an adiabatic approximation of Schrödinger evolution with a time-dependent potential.

**Acknowledgements**

W.C. is partially supported by a Killam Research Fellowship, the Canada Research Chairs Program and NSERC through grant number 238452–11. P.G. is partially supported by the NSF through grant number DMS–0920850. C.S. is partially supported by NSERC through grant number 46179–11. P.G. would like to thank D. Colton for fruitful discussions, and the Institute for Advanced Study (Princeton, NJ) for its hospitality during the academic year 2011–2012. We also thank X. Liu for an analysis of the parametric dependence of the coefficients in § 4, and the accurate numerical calculations of bound states.

## Appendix A. Expansion of Dirichlet–Neumann operators

The first three terms in the Taylor series expansion of (2.12),

$$G(\eta) = \sum_{j=0}^{\infty} G^{(j)}(\eta), \tag{A 1}$$

are given by

$$G^{(0)} = D\tanh(hD), \tag{A 2a}$$

$$G^{(1)} = D\eta D - G^{(0)}\eta G^{(0)}, \tag{A 2b}$$

$$G^{(2)} = -\tfrac{1}{2}(D^2\eta^2 G^{(0)} + G^{(0)}\eta^2 D^2 - 2G^{(0)}\eta G^{(0)}\eta G^{(0)}), \tag{A 2c}$$

where $D = -\mathrm{i}\partial_x$ (so that its Fourier symbol is $k$). The first- and second-order contributions in the Taylor series expansion of (2.13),

$$\begin{pmatrix} G_{11}(\eta,\eta_1) & G_{12}(\eta,\eta_1) \\ G_{21}(\eta,\eta_1) & G_{22}(\eta,\eta_1) \end{pmatrix} = \sum_{m_0,m_1=0}^{\infty} \begin{pmatrix} G_{11}^{(m_0,m_1)}(\eta,\eta_1) & G_{12}^{(m_0,m_1)}(\eta,\eta_1) \\ G_{21}^{(m_0,m_1)}(\eta,\eta_1) & G_{22}^{(m_0,m_1)}(\eta,\eta_1) \end{pmatrix}, \tag{A 3}$$

read

$$\begin{pmatrix} G_{11}^{(0)} & G_{12}^{(0)} \\ G_{21}^{(0)} & G_{22}^{(0)} \end{pmatrix} = \begin{pmatrix} D\coth(h_1D) & -D\,\mathrm{csch}(h_1D) \\ -D\,\mathrm{csch}(h_1D) & D\coth(h_1D) \end{pmatrix}, \tag{A 4}$$

$$\begin{pmatrix} G_{11}^{(10)}(\eta,\eta_1) & G_{12}^{(10)}(\eta,\eta_1) \\ G_{21}^{(10)}(\eta,\eta_1) & G_{22}^{(10)}(\eta,\eta_1) \end{pmatrix} = \begin{pmatrix} D\coth(h_1D)\eta(x)D\coth(h_1D) - D\eta(x)D & -D\coth(h_1D)\eta(x)D\,\mathrm{csch}(h_1D) \\ -D\,\mathrm{csch}(h_1D)\eta(x)D\coth(h_1D) & D\,\mathrm{csch}(h_1D)\eta(x)D\,\mathrm{csch}(h_1D) \end{pmatrix} \tag{A 5}$$

and

$$\begin{pmatrix} G_{11}^{(01)}(\eta,\eta_1) & G_{12}^{(01)}(\eta,\eta_1) \\ G_{21}^{(01)}(\eta,\eta_1) & G_{22}^{(01)}(\eta,\eta_1) \end{pmatrix} = \begin{pmatrix} -D\,\mathrm{csch}(h_1D)\eta_1(x)D\,\mathrm{csch}(h_1D) & D\,\mathrm{csch}(h_1D)\eta_1(x)D\coth(h_1D) \\ D\coth(h_1D)\eta_1(x)D\,\mathrm{csch}(h_1D) & -D\coth(h_1D)\eta_1(x)D\coth(h_1D) + D\eta_1(x)D \end{pmatrix}. \tag{A 6}$$

## Appendix B. Expressions for the dispersion and interaction coefficients

This section gives the expressions for the dispersion and interaction coefficients that appear in the Hamiltonian (3.11) and in the corresponding equations of motion,

$$\begin{aligned} \frac{1}{24}\omega^2(0)'''' = &-\frac{gh^2}{3\rho^2}(\rho-\rho_1)(\rho h + 3\rho_1 h_1)a^-(0)^2 \\ &-\frac{gh}{3\rho^2}\sqrt{\rho_1(\rho-\rho_1)}(2\rho h^2 + 6\rho_1 h h_1 + 3\rho h_1^2)a^-(0)b^-(0) \\ &-\frac{g}{3\rho^2}(\rho^2 h_1^3 + \rho\rho_1 h^3 + 3\rho\rho_1 h h_1^2 + 3\rho_1^2 h^2 h_1)b^-(0)^2, \end{aligned} \tag{B 1}$$

$$\begin{aligned} \kappa = &-\frac{\sqrt{g(\rho-\rho_1)}}{\rho}a^-(0)^3 - 2\frac{\sqrt{g\rho_1}}{\rho}a^-(0)^2 b^-(0) \\ &-\sqrt{\frac{g}{\rho_1}}b^-(0)^3 + \frac{\sqrt{g(\rho-\rho_1)}}{\rho}a^-(0)b^-(0)^2, \end{aligned} \tag{B 2}$$

$$\kappa_1 = \frac{1}{2}\sqrt{g}\,\omega_1^{-1}\left[\frac{1}{\sqrt{\rho-\rho_1}}a^-(0)\,(\sqrt{\rho-\rho_1}G_{11}^{(0)}a^+ - \sqrt{\rho_1}G_{12}^{(0)}b^+)^2\right.$$
$$\times B_0^{-2}(\rho k_0^2 - (\rho-\rho_1)\,(G^{(0)})^2)$$
$$-\frac{\rho_1}{\sqrt{\rho-\rho_1}}a^-(0)k_0^2B_0^{-2}\left(\sqrt{\rho-\rho_1}G^{(0)}a^+ + \frac{\rho}{\sqrt{\rho_1}}G_{12}^{(0)}b^+\right)^2$$
$$-\sqrt{\rho_1}b^-(0)\left(\sqrt{\rho-\rho_1}G^{(0)}B_0^{-1}G_{12}^{(0)}a^+ - \frac{1}{\sqrt{\rho_1}}\{G_{11}^{(0)} - \rho B_0^{-1}\,(G_{12}^{(0)})^2\}b^+\right)^2$$
$$\left.+\frac{1}{\sqrt{\rho_1}}b^-(0)k_0^2\,(b^+)^2\right], \tag{B 3}$$

$$\kappa_2 = \sqrt{g}\,k_0\left[\frac{1}{\sqrt{\rho_1}}b^-(0)\,(b^+)^2 + \sqrt{\rho-\rho_1}b^-(0)B_0^{-1}G_{12}^{(0)}a^+b^+\right.$$
$$+\sqrt{\rho_1}b^-(0)B_0^{-1}(G^{(0)} + G_{11}^{(0)})\,(a^+)^2$$
$$\left.+a^-(0)B_0^{-1}(\sqrt{\rho-\rho_1}G_{11}^{(0)}a^+ - \sqrt{\rho_1}G_{12}^{(0)}b^+)a^+\right], \tag{B 4}$$

$$\kappa_3 = \frac{1}{2}\sqrt{g}\,\omega_1^{-1}\left[\frac{1}{\sqrt{\rho-\rho_1}}a^+(0)\,(\sqrt{\rho-\rho_1}G_{11}^{(0)}a^+ - \sqrt{\rho_1}G_{12}^{(0)}b^+)^2\right.$$
$$\times B_0^{-2}(\rho k_0^2 - (\rho-\rho_1)\,(G^{(0)})^2)$$
$$-\frac{\rho_1}{\sqrt{\rho-\rho_1}}a^+(0)k_0^2B_0^{-2}\left(\sqrt{\rho-\rho_1}G^{(0)}a^+ + \frac{\rho}{\sqrt{\rho_1}}G_{12}^{(0)}b^+\right)^2$$
$$-\sqrt{\rho_1}b^+(0)\left(\sqrt{\rho-\rho_1}G^{(0)}B_0^{-1}G_{12}^{(0)}a^+ - \frac{1}{\sqrt{\rho_1}}\{G_{11}^{(0)} - \rho B_0^{-1}\,(G_{12}^{(0)})^2\}b^+\right)^2$$
$$\left.+\frac{1}{\sqrt{\rho_1}}b^+(0)k_0^2\,(b^+)^2\right], \tag{B 5}$$

$$\kappa_4 = \sqrt{g}\,k_0\left[\frac{1}{\sqrt{\rho_1}}b^+(0)\,(b^+)^2 + \sqrt{\rho-\rho_1}b^+(0)B_0^{-1}G_{12}^{(0)}a^+b^+\right.$$
$$+\sqrt{\rho_1}b^+(0)B_0^{-1}(G^{(0)} + G_{11}^{(0)})\,(a^+)^2$$
$$\left.+a^+(0)B_0^{-1}(\sqrt{\rho-\rho_1}G_{11}^{(0)}a^+ - \sqrt{\rho_1}G_{12}^{(0)}b^+)a^+\right], \tag{B 6}$$

where $B_0 = \rho G_{11}^{(0)} + \rho_1 G^{(0)}$, and

$$a^\pm(0) = \frac{1}{\sqrt{1+d^\pm\,(0)^2}}, \quad b^\pm(0) = \frac{d^\pm(0)}{\sqrt{1+d^\pm\,(0)^2}}, \tag{B 7}$$

with

$$d^\pm(0) = \frac{1}{h\sqrt{\rho_1(\rho-\rho_1)}}\left(\rho_1 h + \frac{1}{2}\rho h_1 - \frac{1}{2}\rho h \pm \frac{1}{2}\rho\sqrt{(h-h_1)^2 + 4\frac{\rho_1}{\rho}hh_1}\right). \tag{B 8}$$

Note that, in the above equations for $\kappa_1$, $\kappa_2$, $\kappa_3$ and $\kappa_4$, the coefficients $\omega_1$, $a^\pm$, $b^\pm$, $G^{(0)}$, $G_{ij}^{(0)}$ and $B_0$ that appear without argument are taken at $k = k_0$.

## Appendix C. Validity of successive approximations

We limit the analysis to the solution in the region $-\infty < x < -A$. Clearly the analysis is similar for the solution on the right half-axis $A < x < +\infty$. Denoting

$k = \sqrt{\lambda}/\delta$, the solution for $x < -A$ has the form

$$u(x) = c\,\mathrm{e}^{-\mathrm{i}kx} + \frac{1}{\delta\sqrt{\lambda}} \int_{-\infty}^{x} \sin[k(x-y)] r(y) u(y)\,\mathrm{d}y. \tag{C 1}$$

Iterating the formula

$$\begin{aligned} u(x) = c\,\mathrm{e}^{-\mathrm{i}kx} &+ \frac{c}{\delta^2} \int_{-\infty}^{x} \frac{\sin[k(x-y)]}{k} r(y) \mathrm{e}^{-\mathrm{i}ky}\,\mathrm{d}y + \cdots \\ &+ c\left(\frac{1}{\delta^2}\right)^m \int_{-\infty}^{x} \cdots \int_{-\infty}^{y_{m-1}} \frac{\sin[k(x-y_1)]}{k} \cdots \frac{\sin[k(y_{m-1}-y_m)]}{k} \\ &\times r(y_1) \cdots r(y_m) \mathrm{e}^{-\mathrm{i}ky_m}\,\mathrm{d}y_1 \cdots \mathrm{d}y_m, \end{aligned} \tag{C 2}$$

we can write

$$u(x) = c \sum_{m=0}^{\infty} T^{(m)}(\mathrm{e}^{-\mathrm{i}kx}), \tag{C 3}$$

with

$$\begin{aligned} T^{(m)}(\mathrm{e}^{-\mathrm{i}kx}) = \left(\frac{1}{\delta^2}\right)^m &\int_{-\infty}^{x} \cdots \int_{-\infty}^{y_{m-1}} \frac{\sin[k(x-y_1)]}{k} \cdots \frac{\sin[k(y_{m-1}-y_m)]}{k} \\ &\times r(y_1) \cdots r(y_m) \mathrm{e}^{-\mathrm{i}ky_m}\,\mathrm{d}y_1 \cdots \mathrm{d}y_m. \end{aligned} \tag{C 4}$$

By simple change of variables, we have the following lemma.

LEMMA C.1.

$$\| T^{(m)}(\mathrm{e}^{-\mathrm{i}kx}) \|_{L^\infty} \leqslant \frac{1}{(m!)^2} \left(\frac{\mathrm{e}^{-A\sqrt{a}}}{\delta^2}\right)^m, \tag{C 5}$$

*where the potential is given by the KdV soliton* $r(x) = -a\,\mathrm{sech}^2(\sqrt{a}x)$ .

Similarly, we can write an expression for the derivative $\partial_x u$ as

$$\partial_x u(x) = -\mathrm{i}kc \sum_{m=0}^{\infty} S^{(m)}(\mathrm{e}^{-\mathrm{i}kx}), \tag{C 6}$$

and have the estimate in the following lemma.

LEMMA C.2.

$$\| S^{(m)}(\mathrm{e}^{-\mathrm{i}kx}) \|_{L^\infty} \leqslant \frac{\sqrt{a}}{k} \frac{m}{(m!)^2} \left(\frac{\mathrm{e}^{-A\sqrt{a}}}{\delta^2}\right)^m. \tag{C 7}$$

LEMMA C.3. *Given a, $\delta$ and $\lambda$ , with the cut-off A large enough, we have*

$$\| T^{(2)} \|_{L^\infty} \ll 1, \quad \| S^{(2)} \|_{L^\infty} \ll 1. \tag{C 8}$$

In order that the truncation of the series at second order suffices for the conclusion regarding the scattering coefficients, we also need that

$$\| T^{(2)} \|_{L^\infty} \ll \| T^{(1)} \|_{L^\infty}, \quad \| S^{(2)} \|_{L^\infty} \ll \| S^{(1)} \|_{L^\infty}. \tag{C 9}$$

For this purpose, we need a lower bound for the first-order approximations, which is obtained by a similar procedure, namely

$$C\frac{\mathrm{e}^{-A\sqrt{a}}}{\delta^2} \leqslant \|T^{(1)}\|_{L^\infty}, \quad C\frac{\mathrm{e}^{-A\sqrt{a}}}{\delta^2} \leqslant k\,\|S^{(1)}\|_{L^\infty}, \tag{C 10}$$

under the assumption that $k \ll 1$. A sufficient condition for (C 9) to hold is that the lower bound for $\|T^{(1)}\|_{L^\infty}$ is larger than the upper bound for $\|T^{(2)}\|_{L^\infty}$, which is again satisfied if $A$ is sufficiently large, given $a$, $\delta$ and $\lambda$.

Turning to the WKB approximation (4.31) in the intermediate region $-A < x < A$, we also find that it is valid if $A$ is sufficiently large.

## Appendix D. Expressions for the matrix $\boldsymbol{M}$ and vector $\boldsymbol{B}$

After simplification of (4.35)–(4.38) in which (4.35) and (4.36) are multiplied by $\mathrm{i}\delta^3/\sqrt{\lambda}$, the system for $\boldsymbol{X} = (b, c, \alpha, \beta)^{\mathrm{T}}$ is set up in matrix form as $\boldsymbol{MX} = \boldsymbol{B}$. To write the expressions for the entries of $\boldsymbol{M}$ and $\boldsymbol{B}$, it is convenient to introduce the notation

$$\widehat{r_A}(\mu) = \int_A^\infty \mathrm{e}^{-\mathrm{i}\mu x} r(x)\,\mathrm{d}x. \tag{D 1}$$

The entries of the column vector $\boldsymbol{B} = [b_1, b_2, b_3, b_4]^{\mathrm{T}}$ are

$$b_1 = -\frac{\mathrm{i}\delta^3}{\sqrt{\lambda}}\,\mathrm{e}^{-2\mathrm{i}kA} + \frac{\delta^2}{2\lambda}[\widehat{r_A}(2k) - \mathrm{e}^{-2\mathrm{i}kA}\widehat{r_A}(0)], \tag{D 2a}$$

$$b_2 = \delta\sqrt{\lambda}\,\mathrm{e}^{-2\mathrm{i}kA} + \frac{1}{2i}[\widehat{r_A}(2k) + \mathrm{e}^{-2\mathrm{i}kA}\widehat{r_A}(0)], \tag{D 2b}$$

$$b_3 = b_4 = 0, \tag{D 2c}$$

where $k = \sqrt{\lambda}/\delta$. The $4 \times 4$ matrix $\boldsymbol{M}$ has the form

$$\boldsymbol{M} = \begin{pmatrix} a_1 & 0 & M_2 & M_1 \\ a_2 & 0 & M_4 & M_3 \\ 0 & a_1 & M_1 & M_2 \\ 0 & a_2 & M_3 & M_4 \end{pmatrix}, \tag{D 3}$$

with

$$a_1 = \frac{\mathrm{i}\delta^3}{\sqrt{\lambda}} - \frac{\delta^2}{2\lambda}[\widehat{r_A}(0) - \mathrm{e}^{-2\mathrm{i}kA}\widehat{r_A}(-2k)], \tag{D 4a}$$

$$a_2 = \delta\sqrt{\lambda} - \frac{1}{2i}[\widehat{r_A}(0) + \mathrm{e}^{-2\mathrm{i}kA}\widehat{r_A}(-2k)], \tag{D 4b}$$

$$M_1 = -\frac{\mathrm{i}\delta^3}{\sqrt{\lambda}}\,[\lambda - r(A)]^{-1/4}\,\mathrm{e}^{\mathrm{i}J/\delta}, \tag{D 5a}$$

$$M_2 = -\frac{\mathrm{i}\delta^3}{\sqrt{\lambda}}\,[\lambda - r(A)]^{-1/4}\,\mathrm{e}^{-\mathrm{i}J/\delta}\mathrm{e}^{-2\mathrm{i}kA}, \tag{D 5b}$$

$$M_3 = \left\{\frac{\mathrm{i}\delta^2}{4}r'(A)\,[\lambda - r(A)]^{-5/4} - \delta\,[\lambda - r(A)]^{1/4}\right\}\mathrm{e}^{\mathrm{i}J/\delta}, \tag{D 5c}$$

$$M_4 = \left\{\frac{\mathrm{i}\delta^2}{4}r'(A)\,[\lambda - r(A)]^{-5/4} + \delta\,[\lambda - r(A)]^{1/4}\right\}\mathrm{e}^{-\mathrm{i}J/\delta}\mathrm{e}^{-2\mathrm{i}kA}, \tag{D 5d}$$

where

$$J = \int_0^A \left[ \sqrt{\lambda - r(s)} - \sqrt{\lambda} \right] \mathrm{d}s. \tag{D 6}$$

## REFERENCES


ALPERS, W. 1985 Theory of radar imaging of internal waves. *Nature* **314**, 245–247.

BAKHANOV, V. V. & OSTROVSKY, L. A. 2002 Action of strong internal solitary waves on surface waves. *J. Geophys. Res.* **107**, 3139.

BASOVICH, A. YA. & BAHANOV, V. V. 1984 Surface wave kinematics in the field of an internal wave. *Izv. Atmos. Ocean Phys.* **20**, 50–54.

BASOVICH, A. YA. & TALANOV, V. I. 1977 Transformation of short surface waves on inhomogeneous currents. *Izv. Atmos. Ocean Phys.* **13**, 514–519.

BENJAMIN, T. B. & BRIDGES, T. J. 1997 Reappraisal of the Kelvin–Helmholtz problem. I. Hamiltonian structure. *J. Fluid Mech.* **333**, 301–325.

BOURGAULT, D. & KELLEY, D. E. 2003 Wave-induced boundary mixing in a partially mixed estuary. *J. Mar. Res.* **61**, 553–576.

CAPONI, E. A., CRAWFORD, D. R., YUEN, H. C. & SAFFMAN, P. G. 1988 Modulation of radar backscatter from the ocean by a variable surface current. *J. Geophys. Res.* **93**, 12249–12263.

CHADAN, K., COLTON, D., PAIVARINTA, L. & RUNDELL, W. 1997 *An Introduction to Inverse Scattering and Inverse Spectral Problems*. SIAM.

CRAIG, W., GUYENNE, P. & KALISCH, H. 2005 Hamiltonian long-wave expansions for free surfaces and interfaces. *Commun. Pure Appl. Maths* **58**, 1587–1641.

CRAIG, W., GUYENNE, P. & SULEM, C. 2010 A Hamiltonian approach to nonlinear modulation of surface water waves. *Wave Motion* **47**, 552–563.

CRAIG, W., GUYENNE, P. & SULEM, C. 2011 Coupling between internal and surface waves. *Nat. Hazards* **57**, 617–642.

CRAIG, W., SCHANZ, U. & SULEM, C. 1997 The modulational regime of three-dimensional water waves and the Davey–Stewartson system. *Ann. Inst. Henri Poincaré (C) Nonlin. Anal.* **14**, 615–667.

DJORDJEVIC, V. D. & REDEKOPP, R. G. 1977 On two-dimensional packets of capillary-gravity waves. *J. Fluid Mech.* **79**, 703–714.

DONATO, A. N., PEREGRINE, D. H. & STOCKER, J. R. 1999 The focusing of surface waves by internal waves. *J. Fluid Mech.* **384**, 27–58.

EVANS, W. A. B. & FORD, M. J. 1996 An integral equation approach to internal (2-layer) solitary waves. *Phys. Fluids* **8**, 2032–2047.

FUNAKOSHI, M. & OIKAWA, M. 1983 The resonant interaction between a long internal gravity wave and a surface gravity wave packet. *J. Phys. Soc. Japan* **56**, 1982–1995.

GARGETT, A. E. & HUGHES, B. A. 1972 On the interaction of surface and internal waves. *J. Fluid Mech.* **52**, 179–191.

GASPAROVIC, R. F., APEL, J. R. & KASISCHKE, E. S. 1988 An overview of the SAR internal wave signature experiment. *J. Geophys. Res.* **93**, 12304–12316.

GEAR, J. & GRIMSHAW, R. 1984 Weak and strong interactions between internal solitary waves. *Stud. Appl. Maths* **70**, 235–258.

HASHIZUME, Y. 1980 Interaction between short surface waves and long internal waves. *J. Phys. Soc. Japan* **48**, 631–638.

HELFRICH, K. R. & MELVILLE, W. K. 2006 Long nonlinear internal waves. *Annu. Rev. Fluid Mech.* **38**, 395–425.

KAWAHARA, T., SUGIMOTO, N. & KAKUTANI, T. 1975 Nonlinear interaction between short and long capillary-gravity waves. *J. Phys. Soc. Japan* **39**, 1379–1386.

LEE, K.-J., HWUNG, H.-H., YANG, R.-Y. & SHUGAN, I. V. 2007 Stokes wave modulation by internal waves. *Geophys. Res. Lett.* **34**, L23605.

LEWIS, J. E., LAKE, B. M. & KO, D. R. S. 1974 On the interaction of internal waves and surface gravity waves. *J. Fluid Mech.* **63**, 773–800.

LONGUET-HIGGINS, M. S. & STEWART, R. W. 1964 Radiation stress in water waves, a physical discussion with applications. *Deep-Sea Res.* **11**, 529–562.

MA, Y.-C. 1983 A study of resonant interactions between internal and surface waves based on a two-layer fluid model. *Wave Motion* **5**, 145–155.

MARSTON, C. C. & BALINT-KURTI, G. G. 1989 The Fourier grid Hamiltonian method for bound state eigenvalues and eigenfunctions. *J. Chem. Phys.* **91**, 3571–3576.

OSBORNE, A. R. & BURCH, T. L. 1980 Internal solitons in the Andaman Sea. *Science* **208**, 451–460.

PĂRĂU, E. & DIAS, F. 2001 Interfacial periodic waves of permanent form with free-surface boundary conditions. *J. Fluid Mech.* **437**, 325–336.

PERRY, B. R. & SCHIMKE, G. R. 1965 Large-amplitude internal waves observed off the northwest coast of Sumatra. *J. Geophys. Res.* **70**, 2319–2324.

PETERS, A. S. & STOKER, J. J. 1960 Solitary waves in liquids having non-constant density. *Commun. Pure Appl. Maths* **13**, 115–164.

PHILLIPS, O. M. 1966 *The Dynamics of the Upper Ocean*. Cambridge University Press.